

Article

Active Dielectric Window: A New Concept of Combined Acoustic Emission and Electromagnetic Partial Discharge Detector for Power Transformers

Wojciech Sikorski 

Institute of Electrical Power Engineering, Poznan University of Technology, Piotrowo 3A, 60-965 Poznan, Poland; wojciech.sikorski@put.poznan.pl; Tel.: +48-061-665-2035

Received: 23 November 2018; Accepted: 24 December 2018; Published: 29 December 2018



Abstract: The detection and location of partial discharge (PD) is of great significance in evaluating the insulation condition of power transformers. This paper presents an active dielectric window (ADW), which is a new concept of combined acoustic emission (AE) and electromagnetic PD detector intended for assembly in a transformer's inspection hatch. The novelty of this design lies in the fact that all structural components of an ultrasonic transducer, i.e., the matching and backing layer, an active piezoelectric element with electrodes, and electrical leads, were built into a dielectric window. Due to the fact that its construction was optimized for work in mineral oil, it is characterized by much higher sensitivity of PD detection than a general-purpose AE sensor mounted outside a transformer tank. Laboratory tests showed that the amplitude of the AE pulses generated by creeping discharges, which were registered by the ADW, was around five times higher on average than the pulses registered by a commonly used contact transducer. A possibility of simultaneous detection of acoustic and electromagnetic pulses (with an integrated ultra-high frequency (UHF) antenna) is an important advantage of the ADW. It allows for an increase in the reliability of PD detection, the accuracy of defect location, and the effectiveness of disturbance identification. This paper describes in detail the applied methods of designing and modeling the ADW components, the manufacturing process of the prototype construction, and the results of preliminary laboratory tests, in which the detector's sensitivity as well as the efficiency of the PD source location were evaluated.

Keywords: partial discharge (PD); power transformer diagnostics; condition monitoring; acoustic emission (AE); PD source location; UHF antenna

1. Introduction

Partial discharge (PD) detection based on an acoustic emission method is an important and widely applied technique for diagnostics of high voltage (HV) power electrical equipment, mainly due to such advantages as (1) the possibility of conducting measurements without the necessity to de-energize an HV device, (2) the possibility of precise location of PD sources, (3) the ease of adjustment to working in an online monitoring mode, or (4) the possibility of identifying the type of insulation defect [1]. Unfortunately, besides unquestionable advantages, the acoustic emission (AE) method has one basic weakness: The relatively low sensitivity of PD detection. This results directly from the physical nature of the PD phenomenon, because only a small part of the energy (estimated at about 5%) of a PD current pulse is transformed into mechanical energy in the form of acoustic emission waves, being mostly ultrasounds in the range from 20 to 300 kHz. The remaining part of electrical energy is transformed mainly into thermal and chemical energy [1–3].

Usually, with the AE method, contact piezoelectric transducers, commonly available on the market, are used. They consist of three main parts: Piezoelectric crystal, a matching layer (wear plate), and a

backing layer. The ancillary components in an ultrasonic transducer comprise the housing, optional acoustic insulation layers, and electrical leads with a connector (Figure 1). For power transformer diagnostics, the users typically choose transducers with a resonant frequency for longitudinal waves of either 60 kHz or 150 kHz [1,2,4,5]. Transducers with a resonant frequency of 60 kHz guarantee higher sensitivity of PD detection. However, due to the possibility of disturbance occurrences during field measurements, they are mainly preferred for factory and laboratory use. For that reason, most users choose the 150 kHz transducers, which are a compromise between acceptable PD detection sensitivity and immunity to disturbances [2,6–9].

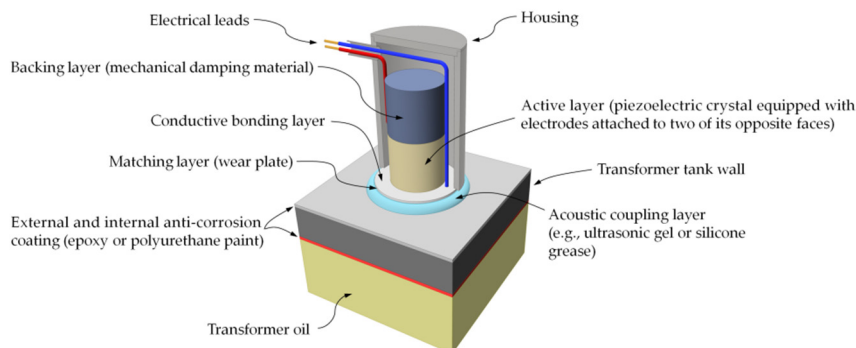


Figure 1. Schematic diagram of a contact piezoelectric transducer mounted on the surface of a power transformer tank.

Ultrasonic transducers are mounted on the external surface of a transformer tank. Unfortunately, this is the main reason for low PD detection sensitivity using the AE method. Assuming that the acoustic impedance of mineral oil is equal to $Z_{oil} = 1.28$ MRayl, and for a steel transformer tank $Z_{steel} = 46.2$ MRayl, then from Equation (1) for transmission coefficient T , it follows that at most 10.5% of AE wave energy passes through the transformer tank wall to the transducer, and the remaining 89.5% is reflected [10]:

$$T = \frac{4Z_{oil}Z_{steel}}{(Z_{oil} + Z_{steel})^2} \quad (1)$$

Between the metal transformer tank wall and the piezoelectric element, there is a transducer's wear plate, a front matching layer made of a material such as high-density alumina or an alumina/epoxy composite. Moreover, the internal and external tank surface is covered with anticorrosive epoxy or polyurethane paint. In effect, the wave may be reflected again due to acoustic impedance mismatch at the interface of the transducer's front material and painted steel wall.

For long-term installations (e.g., online AE monitoring systems), permanent mounting of ultrasonic transducers is realized by using magnetic holders [2,11–13]. Although they provide a very stable and durable mechanical coupling between the transducer and the transformer tank, the magnetic holders can also slightly reduce the sensitivity and bandwidth of the transducer [2]. To ensure an efficient transmission of the AE signal from the tank wall to the piezoelectric element, a wear plate is covered with a film of acoustic couplant (usually glycerin, silicone grease, or propylene glycol) approximately 0.5 mm thick. In the case of long-term installations, an acoustic couplant may be exposed to extreme weather conditions, and after some time it becomes naturally degraded and loses its initial properties. It should be underlined that complete loss and even a too thin layer of acoustic couplant can dramatically decrease the transducer's sensing capabilities.

Contact ultrasonic transducers mounted on the external walls of a transformer tank may be exposed to a number of types of disturbances, such as environmental noises (e.g., rain, hail, thunderstorms, sandstorms, wind), oil circulating pumps and fan noises, or acoustic signals produced by switching operations in a substation. Therefore, without correlation between the acoustic and electromagnetic signals (e.g., using a high-frequency current transformer or internal ultra-high

frequency (UHF) antenna), it is practically impossible to effectively and reliably distinguish between the PD and noise signals [14–16].

One may also find solutions where in order to increase the detection sensitivity of AE signals from PD, the ultrasonic transducer is inserted into the interior of a power transformer tank. In this case, the amplitude of recorded AE signals can be even several times higher than for contact transducers. In References [17,18], the construction of a power transformer monitoring system with a combined PD detector consisting of a piezoelectric ultrasonic transducer and a capacitive sensor was presented. The ultrasonic transducer was embedded inside the epoxy cover equipped with a screw with which the transducer was coaxially attached to the dielectric plate. In Reference [19], an interesting design of a combined PD detector, containing in its housing an ultrasonic transducer and a UHF antenna, was presented. The active elements of the detector were embedded at the end of the metal rod, which was inserted into the interior of the power transformer tank through a DN50 or DN80 oil drain valve.

This paper presents a new concept, the active dielectric window (ADW). The idea for this solution lay in the fact that at least one active element in the form of piezoelectric ceramics and remaining structures of an ultrasonic transducer constitute an integral part of a dielectric window. By placing the UHF antenna in the window, we obtained a combined ultrasonic and electromagnetic PD detector.

The general conceptual assumptions of the ADW, as well as its advantages, are in detail discussed in Section 2. In the subsequent sections of the paper, the following issues are described: The applied methods of designing and modeling active dielectric window components (Section 3), the production process of the prototype construction (Section 4), and the results of preliminary laboratory tests, in which the sensitivity of the detector and the possibilities for its application for PD source location were evaluated (Section 5).

2. General Conceptual Assumptions of the Active Dielectric Window for PD Online Monitoring and Location

Power transformer and reactor tanks, as well as gas-insulated substation (GIS) and gas-insulated line (GIL) housings, are factory-equipped in the inspection hatches. It is typically a round through-hole, around which there is a steel flange with a gasket or O-ring and a cover mounted to the flange with assembly bolts.

The hole in the inspection hatch can be plugged with an element made of a solid dielectric (e.g., high-density alumina ceramics), which in the literature is known as a "dielectric window" [20,21]. A task of the dielectric window is to enable the registration of electromagnetic (EM) waves generated by PD using the electromagnetic detectors, mostly very high frequency (VHF) and ultrahigh frequency (UHF) antennas (Figure 2). This is possible because the dielectric window, contrary to the metal housing of a device, is not a barrier for EM waves of radio frequencies generated by partial discharge.

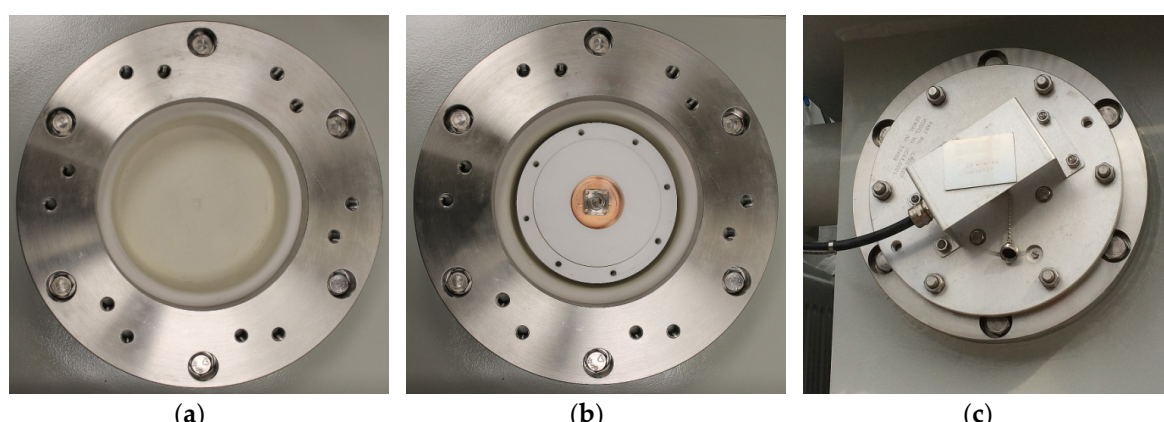


Figure 2. Inspection hatch in the power transformer tank: (a) Dielectric window; (b) ultrahigh frequency (UHF) antenna (partial discharge (PD) detector) installed in the dielectric window; (c) inspection hole cover with electronics in the enclosure.

The design of the ADW was based on four piezoelectric elements equipped in electrodes, electrical leads, and matching and backing layers. The schematic diagram of the active dielectric window is shown in Figure 3.

The ADW was designed to perform two functions simultaneously, that of a detector of AE pulses generated by partial discharges and that of a dielectric window used for UHF antenna mounting.

The possibility of simultaneous application of two different diagnostic techniques (i.e., the AE method and the UHF electromagnetic method) allows an increase in the reliability of PD detection and the effectiveness of disturbance identification, both acoustic and EM (e.g., corona discharge, switching operations at substations, on-load tap-changer operations, Barkhausen noise).

The proposed solution has other advantages as well. In regard to the fact that the ultrasonic transducer is placed inside the tank, its metal wall is not a barrier for ultrasonic waves, as it is in the case of standard, tank-mounted AE sensors. Additionally, the application of a specially designed matching layer in a transducer enables a transfer of acoustic energy from mineral oil (as well as other insulating liquids such as natural or synthetic esters [22,23]) to a piezoelectric element. As a result, the ADW should assure higher sensitivity of detection of AE pulses generated by PDs than a conventional, contact piezoelectric transducer.

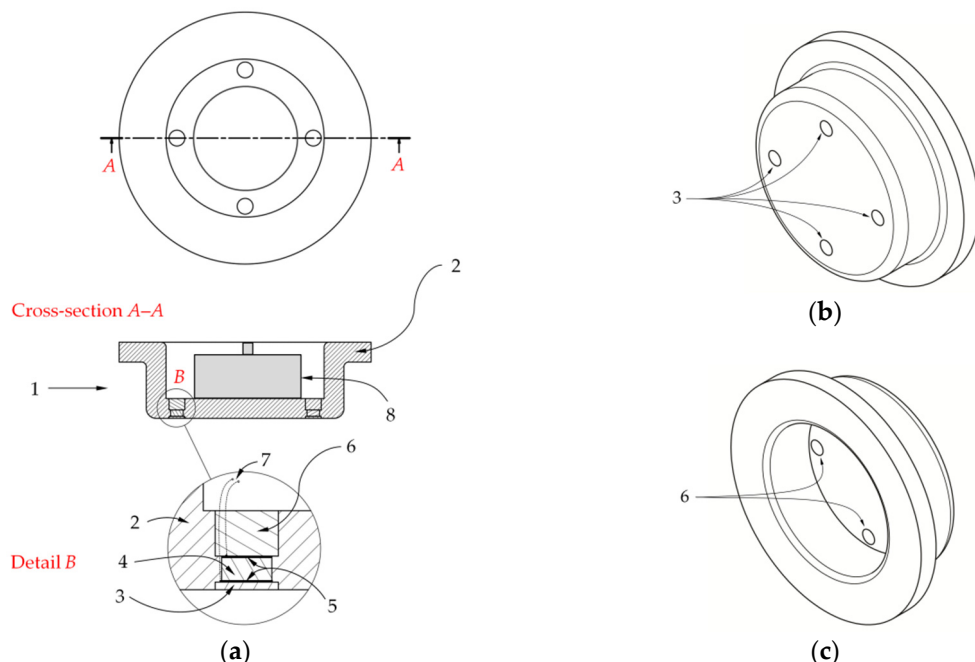


Figure 3. Schematic diagram of the active dielectric window: (a) Top and cross-sectional view; (b) isometric view of the front and (c) the back side of the active dielectric window (ADW). Indications of structural elements: 1 = active dielectric window; 2 = ceramics; 3 = matching layer; 4 = piezoelectric crystal; 5 = electrodes; 6 = backing layer; 7 = electrical leads; 8 = UHF antenna (PD detector).

An active dielectric window, depending on the intended use, may be produced in various configurations. For online PD monitoring, the simplest configuration with one ultrasonic transducer and a UHF antenna is sufficient. It allows analysis of the intensity of a PD using two methods simultaneously. Apart from discharge detection and monitoring, the ADW may also be used for spatial location of PD sources. For this task, an ADW configuration with at least three ultrasonic transducers and a UHF antenna was intended. PD location is performed using the time difference of arrival (TDOA) technique, which is based on the measurement of delays in the arrival of the AE signal to the ultrasonic transducer relative to that registered by the UHF antenna [24]. To estimate the position of the PD source, it is necessary to register time waveforms of discharges simultaneously with the UHF antenna and three ultrasound transducers. The acquisition of PD waveforms is triggered

by a signal coming from the UHF antenna. In turn, in the ADW configuration with four ultrasonic transducers, for location of the PD sources there is no need for the UHF antenna mounting, because time delays are then measured relative to the transducer, which is first to register the pulse (it is a so-called "all-acoustic PD location") [16].

The way the ADW is mounted in the inspection hatch is identical to the case of a standard dielectric window (Figure 4). Ensuring adequate tightness in order to avoid undesired oil leaks has a fundamental meaning. For that reason, at least two gaskets must be used, where a highly conductive shielding gasket is placed between the welded flange and the inspection hole cover.

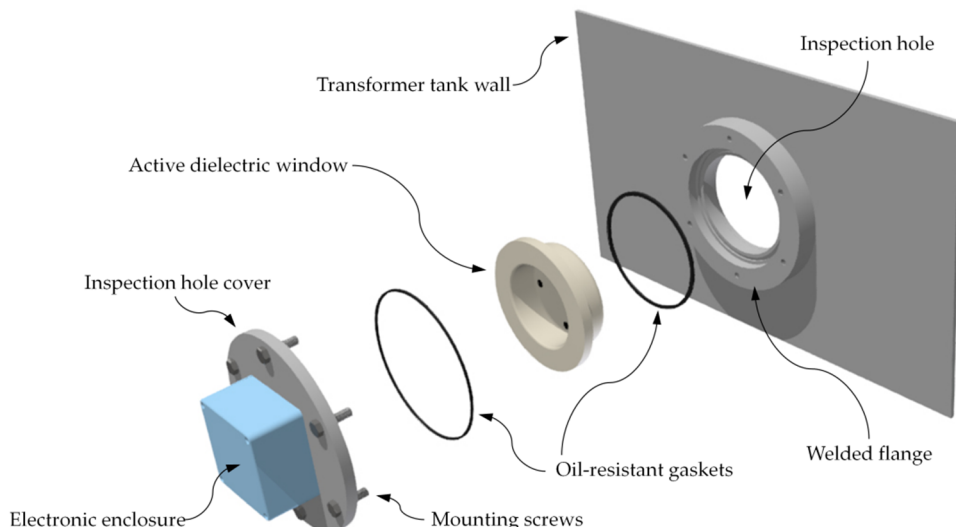


Figure 4. The method of assembling the active dielectric window in the inspection hole.

3. Designing and Modeling of Active Dielectric Window Components

3.1. Mathematical Modeling of Piezoelectric Transducer Structures

Various mathematical models for ultrasonic transducers based on piezoceramic materials have been around for a long time and allow for significantly simplifying and accelerating the design process. A fundamental issue when designing an ultrasonic transducer is the knowledge of the piezoceramic behavior regarding two closely interacting parts: The front/back mechanical side of the ceramic and the electrical part. This electromechanical interaction was first introduced in the form of electrical equivalent circuits by Mason [25]. The developed model, based on network theory, separated the piezoceramic element into an electrical port and two (left and right) acoustic ports through the use of virtual concepts such as negative capacitance and electromechanical transformers. This allowed for describing the behavior of one-dimensional vibrations of a piezoceramic plate, but the introduction of "unphysical" elements into the model has become a source of criticism. Redwood [26] showed that this negative capacitance could be transformed onto the acoustic side of the transformer and treated like a length of acoustic line. Unfortunately, from a physics point of view, the model was still imperfect. Krimholtz, Leedom, and Matthaei [27] developed a new alternative model (commonly referred to as the KLM model), which removed circuit elements between the top of the transducer and the node of the acoustic transmission line. The general structure of the KLM model is shown in Figure 5.

In the KLM model, V_{IN} and I_{IN} are respectively the voltage and current applied to the piezoceramic that produces the resulting acoustic forces F_1 and F_2 . The variables U_1 and U_2 symbolize the particle velocities at the respective faces of the piezoelectric crystal. The particle velocities inside the crystal are denoted by V_B and V_M , where the subscript B indicates the backward-traveling acoustic waves propagating toward the backing layer, and the subscript M indicates the forward-traveling acoustic waves propagating toward the matching layer (the plus and minus signs in the superscript mean the left and right halves of the piezoelectric crystal, respectively).

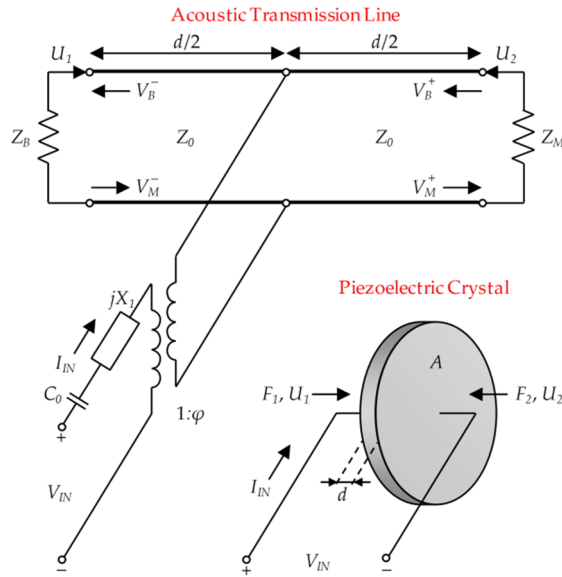


Figure 5. General structure of the Krimholtz, Leedom, and Matthaei (KLM) model of the piezoelectric transducer.

The input parameters include the thickness of the piezoelectric material d , the area of the electrodes A , and the acoustic impedances of the main transducer elements: The piezoelectric crystal Z_0 , backing layer Z_B , and matching layer Z_M . Furthermore, the model consists of input electrical reactance X_1 and input capacitance C_0 . The acoustical side of the KLM model is coupled to the electrical side by a transformer with a turns ratio $(1:\varphi)$. This transformer converts the electrical signal into the appropriate acoustic values. The equations for these parameters are given below:

$$Z_0 = \rho c A = A \sqrt{\rho c_{33}^D}, \quad (2)$$

$$C_0 = \frac{\varepsilon_{33}^S A}{d}, \quad (3)$$

$$X_1 = \frac{h_{33}^2 A}{\omega^2 Z_0} \sin\left(\frac{\omega d}{c}\right), \quad (4)$$

$$\varphi = \frac{\omega Z_0}{2h_{33} \sin(\omega d / 2c)}, \quad (5)$$

$$h_{33} = k_t \sqrt{c_{33}^D / \varepsilon_{33}^S}, \quad (6)$$

where ρ is the density of the piezoceramic material (kg/m^3), c is the velocity of longitudinal acoustic waves (m/s), c_{33}^D is the elastic stiffened for constant electric displacement (N/m^2), ε_{33}^S is the clamped (high-frequency) dielectric constant, φ is the electromechanical transformer ratio of the KLM model, h_{33} is the piezoelectric constant (V/m), and k_t is the electromechanical coupling factor.

Based on the value of the acoustic impedance (in Rayl or $\text{Pa}\cdot\text{s}/\text{m}^3$) of piezoelectric crystal Z_0 , matching layer Z_M , and backing layer Z_B , the input impedances for both layers can be calculated as follows:

$$Z_{IN,M} = Z_0 \frac{Z_M + jZ_0 \tan(\omega d / 2c)}{Z_0 + jZ_M \tan(\omega d / 2c)}, \quad (7)$$

$$Z_{IN,B} = Z_0 \frac{Z_B + jZ_0 \tan(\omega d / 2c)}{Z_0 + jZ_B \tan(\omega d / 2c)}. \quad (8)$$

According to the transmission line theory, the value of the input impedance of the electrical two-port can be determined from Equation (9):

$$Z_{IN} = \frac{1}{j\omega C_0} + jX_1 + \frac{Z_a}{\varphi^2}, \quad (9)$$

where Z_a is the impedance seen looking into the acoustic transmission line,

$$Z_a = \frac{Z_{IN,M}Z_{IN,B}}{Z_{IN,M} + Z_{IN,B}}. \quad (10)$$

Z_{IN} corresponds to the real impedance measured by the impedance analyzer. The minimum impedance frequency on the $Z(f)$ plot is the resonant frequency, at which the piezoceramic element vibrates most readily and most efficiently converts the electrical energy into mechanical energy. In turn, the maximum impedance frequency is also the antiresonance frequency.

In order to determine the pressure radiated by the ultrasonic transducer, which is excited by the voltage V_{IN} , it is necessary to determine the particle velocities U_1 and U_2 :

$$U_1 = -\frac{I_{IN}}{\varphi} \frac{\left(e^{\frac{jkd}{2}} - \Gamma_M e^{-\frac{jkd}{2}}\right)}{e^{jkd} - \Gamma_B \Gamma_M e^{-jkd}} (1 + \Gamma_B) \quad (11)$$

$$U_2 = -\frac{I_{IN}}{\varphi} \frac{\left(\Gamma_B e^{-\frac{jkd}{2}} - e^{\frac{jkd}{2}}\right)}{e^{jkd} - \Gamma_B \Gamma_M e^{-jkd}} (1 + \Gamma_M) \quad (12)$$

where k is the wave number in the piezoelectric crystal, and Γ_B and Γ_M are the current transmission coefficients given by

$$\Gamma_B = \frac{Z_0 - Z_B}{Z_0 + Z_B} \quad (13)$$

$$\Gamma_M = \frac{Z_0 - Z_M}{Z_0 + Z_M} \quad (14)$$

Replacing I_{IN} with V_{IN} and solving for the pressure wave leaving the surface of the piezoelectric crystal gives

$$P_1(\omega) = \frac{Z_B V_{IN}(\omega)}{\varphi Z_{IN}} \frac{\left(e^{\frac{jkd}{2}} - \Gamma_M e^{-\frac{jkd}{2}}\right)}{e^{jkd} - \Gamma_B \Gamma_M e^{-jkd}} (1 + \Gamma_B) \quad (15)$$

$$P_2(\omega) = \frac{Z_M V_{IN}(\omega)}{\varphi Z_{IN}} \frac{\left(\Gamma_B e^{-\frac{jkd}{2}} - e^{\frac{jkd}{2}}\right)}{e^{jkd} - \Gamma_B \Gamma_M e^{-jkd}} (1 + \Gamma_M), \quad (16)$$

where $P_1(\omega)$ and $P_2(\omega)$ are the pressure waves radiated from the back and front faces of the piezoelectric crystal, respectively. The pulse–echo response can be calculated using the inverse fast Fourier transform (IFFT) of the pressure to generator voltage (PGV) transfer function. The PGV is a function that allows the determination of the pressure propagated from the piezoelectric crystal to the matching layer and subsequently to the medium:

$$\frac{P_m}{P_{in,front}} = \prod_{n=1}^{n=N} \frac{Z_{in,n+1}}{Z_{in,n+1} \cos\left(\frac{\omega d}{2c}\right) + j \sin Z_n \sin\left(\frac{\omega d}{2c}\right)} \text{ if } N \geq 1, \quad (17)$$

where P_m is the pressure propagated in the medium, $P_{in,front}$ is the input pressure from the first front layer, Z_n is the acoustic impedance of the front layer under consideration, and $Z_{in,n+1}$ is the input impedance of the following layer.

All structures of the ultrasonic transducer used for building the prototype of the active dielectric window were designed based on the calculations and simulations performed with the KLM model.

3.2. Matching and Backing Layers

The matching layer in the ultrasonic transducer performs a similar function as the antireflection layer applied to the surface of lenses and other optical devices to reduce light reflection. This element enables acoustic emission wave transfer from a medium, in which the transducer is in contact with the piezoelectric crystal. The greater the role of the matching layer, the bigger the difference between acoustic impedance of the piezoelectric crystal and the ultrasonic medium is.

If we assume that Z_0 is an acoustic impedance of piezoelectric material, Z_{oil} is an acoustic impedance of transformer oil, and Z_M is an acoustic emission of a matching layer with thickness l (in which the wavelength at the frequency of interest is λ_l), then the transmission coefficient T for propagation from the transformer oil to the piezoelectric crystal at normal incidence is given as

$$T = \frac{4Z_0Z_{oil}}{(Z_0 + Z_{oil})^2 \cos^2\left(\frac{2\pi l}{\lambda_l}\right) + \left(Z_M + \frac{Z_0Z_{oil}}{Z_M}\right)^2 \sin^2\left(\frac{2\pi l}{\lambda_l}\right)}. \quad (18)$$

Transmission coefficient T takes values from the range between 0 and 1. When $T = 1$, theoretically lossless transmission of acoustic energy from ultrasonic medium to the piezoelectric crystal occurs. In order to meet this condition, the thickness of the matching layer l has to be equal to $\lambda/4$, and then Equation (18) reduces to the form

$$T = \frac{4Z_0Z_{oil}}{\left(Z_M + \frac{Z_0Z_{oil}}{Z_M}\right)^2}. \quad (19)$$

Equation (19) is equal to 1 if the acoustic impedance of the matching layer is the geometric mean of the impedances of transformer oil and the piezoelectric material,

$$Z_M = \sqrt{Z_0Z_M}. \quad (20)$$

Assuming the acoustic impedance of the chosen piezoelectric material equals 31 MRayl, and mineral oil is ~ 1.28 MRayl (at a temperature of 25°C), then the optimal value of matching layer acoustic impedance should total 6.30 MRayl. The material used for its manufacturing ought to be oil-resistant, mechanically durable, and resistant to temperature changes. Unfortunately, acoustic impedance of all durable and chemically resistant plastics, such as polyamide (PA6 or glass fiber-reinforced PA66), acrylonitrile butadiene styrene (ABS), or polyoxymethylene (POM), is definitely too low (< 4 MRayl). To overcome the limitation of the available materials, base resins such as epoxies or polyurethanes are often filled with high-velocity (e.g., alumina, $v \approx 10,500$ m/s) or high-density (e.g., tungsten, $\rho \approx 19,250$ kg/m³) powders to fabricate 0–3 composites with the required properties. The elastic properties of such a two-phase composite can be estimated using the Devaney and Levine model, which is based on a self-consistent formulation of multiple-scattering theory [28]. According to this model, the bulk modulus K and the shear modulus G of the composite are given by Equations (21) and (22):

$$K = K_1 + \varphi_2 \frac{(3K + 4G)(K_2 - K_1)}{3K + 4G + 3(K_2 - K_1)} \quad (21)$$

$$G = G_1 + \varphi_2 \frac{5G(3K + 4G)(G_2 - G_1)}{G(15K + 20G) + 6(K + 2G)(G_2 - G_1)} \quad (22)$$

where K_1 , G_1 , K_2 , and G_2 are the bulk and shear moduli of the matrix (epoxy) and powdered material (filler), respectively. The density of a two-phase composite material is calculated as the volume averaged density,

$$\rho = \varphi_1\rho_1 + \varphi_2\rho_2 \quad (23)$$

where $\varphi_1, \rho_1, \varphi_2, \rho_2$ are the volume fractions and densities of the epoxy and filler, respectively. The longitudinal velocity V_L and shear velocity V_S of the sound wave are directly related to the mechanical parameters K, G , and ρ of the composite:

$$V_L = \sqrt{\frac{K + \frac{4}{3}G}{\rho}} \quad (24)$$

$$V_S = \sqrt{\frac{G}{\rho}}. \quad (25)$$

Finally, the acoustic impedance for the longitudinal sound wave can be calculated as follows:

$$Z_L = \rho V_L. \quad (26)$$

The acoustic impedance values of epoxy/alumina and epoxy/tungsten composites were calculated from Equations (21)–(26) and are presented in Figures 6 and 7. The parameters used for calculations are collected in Table 1.

Table 1. Properties of the materials used to design the matching and backing layer of an ultrasonic transducer.

Parameter	Material			Symbol	Unit
	Epoxy	Alumina Powder	Tungsten Powder		
Density	1094 ^a	3670	19250	ρ	kg/m ³
Bulk modulus	5.1	165	310	K	GPa
Shear modulus	1.5	124	161	G	GPa
Longitudinal velocity	2550	9487	5221	V_L	m/s
Shear velocity	1174	5813	2892	V_S	m/s
Acoustic impedance	2.79	34.8	100.5	Z	MRayl
Particle size	N/A	1	0.6–1	D	μm
Purity	N/A	≥99.9	≥99.9 ^b	-	%

^a At 25 °C; ^b based on trace metals analysis.

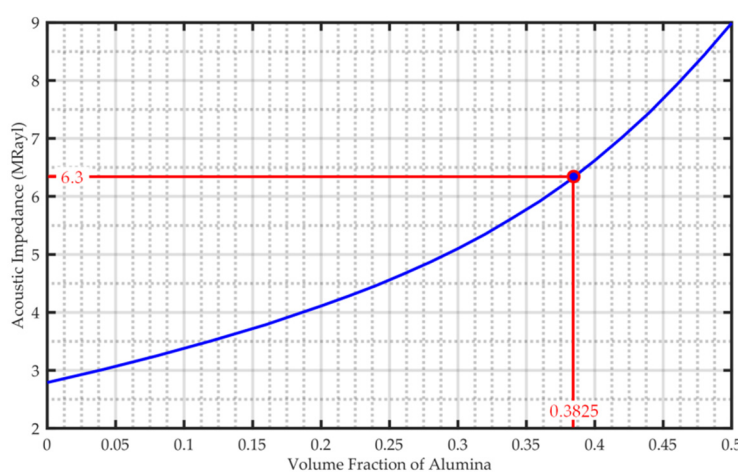


Figure 6. Effect of alumina volume fraction on acoustic impedance of a composite material.

The characteristics presented in Figures 6 and 7 show that for the formation of composite materials with an acoustic impedance equal to 6.3 MRayl, one should use approximately 0.16 pu volume fraction of tungsten or 0.38 pu volume fraction of alumina powder. Obviously, regarding low

attenuation, the alumina powder is a proper material for manufacturing the matching layer. In turn, an epoxy/tungsten composite, due to high attenuation, is an ideal material for manufacturing the damping layer. In the case of the described PD detector, the backing layer performs four functions: (1) It loads the piezoelectric element, which contributes to reducing its resonance (quickly dampening vibrations), (2) it absorbs the backward-directed ultrasound energy and attenuates the acoustic signals from the housing, and (3) it extends the bandwidth.

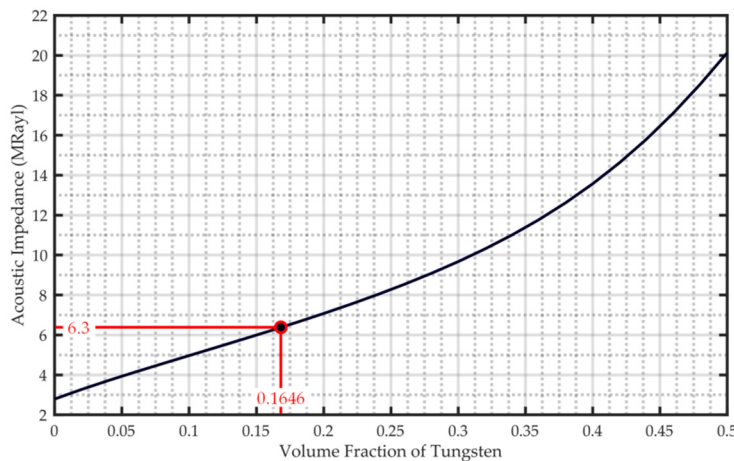


Figure 7. Effect of tungsten volume fraction on acoustic impedance of a composite material.

3.3. Piezoelectric Element

A piezoelectric element performs the function of a receiver (or transmitter) of ultrasonic signals in a transducer. It is typically made in the form of a disc, cylinder, or ring, and its upper and bottom surface are covered by a thin layer of conductive material, which performs the function of an electrode.

In the proposed ADW solution, a disc made of high-purity lead zirconate titanate (PZT) is an active element. The properties of the ceramics used in this study correspond to the general properties of the PZT-5A (Table 2).

Table 2. Properties of the piezoelectric ceramic used.

Parameter	Symbol	Value	Unit
Relative dielectric constant	K^T	1900	-
Electromechanical coupling coefficients:			
Longitudinal coupling coefficient	k_{33}	0.72	-
Transverse coupling coefficient	k_{31}	0.36	-
Shear coupling coefficient	k_{15}	0.68	-
Planar coupling coefficient	k_p	0.63	-
Thickness coupling factor	k_t	0.49	-
Piezoelectric charge constants:			
Induced strain in direction 3 per unit electric field	d_{33}	400	m/V^3
Induced strain in direction 1 per unit electric field applied in direction 3	d_{31}	175	m/V^3
Induced shear strain about direction 2 per unit electric field applied in direction 1	d_{15}	590	m/V^3
Dielectric dissipation factor (dielectric loss) ¹	$\tan \sigma$	≤ 2.00	%
Frequency constants:			
Frequency constant for thickness vibration mode	N_T	2040	$\text{Hz}\cdot\text{m}$
Frequency constant for planar vibration mode	N_P	1980	$\text{Hz}\cdot\text{m}$
Frequency constant for longitudinal vibration mode	N_L	1500	$\text{Hz}\cdot\text{m}$
Curie point ²	T_C	360	$^\circ\text{C}$
Density	ρ	7600	kg/m^3

¹ At 1 kHz, low field; ² maximum operating temperature = Curie point/2; ³ 10^{-12} C/N .

3.4. Frequency Response Modeling of the Piezoelectric Transducer

When starting the frequency response modeling, as a reference point an acoustic emission sensor type PAC R15D (Physical Acoustics, Princeton, USA) was selected, with a resonance frequency of 150 kHz. It has a very good sensitivity and frequency response over the range of 50–400 kHz. The R15D is a differential sensor designed for applications where high-background electrical noise is a major concern. Currently, the R15 series family of AE sensors is one of the most commonly used piezoelectric transducers for PD detection in power transformers.

For designing the transducer components, the following assumptions were made:

- The first resonance frequency should be similar to the PAC R15D sensor, approximately 150 kHz;
- The bandwidth should range between ~100 and ~300 kHz, with a central frequency of ~200 kHz;
- The frequency response curve in the working frequency range ought to be possibly the flattest;
- To improve the efficiency of energy transmission of the acoustic signal from the oil to the piezoelectric element, the acoustic impedance of the matching layer should total 6.3 MRayl;
- Because it was earlier assumed that the standard window made of ceramics would have a thickness of 20 mm, then therefore the height of the piezoelectric element should not exceed 15 mm (the remaining space was intended for matching and backing layers).

The assumed resonance frequency and bandwidth in the above specification are compliant with the IEC [11] (p. 28) and IEEE [2] (p. 12) recommendations regarding the selection of AE sensors for the detection of partial discharges in power transformers.

Frequency response curve modeling was made using the KLM model, a detailed description of which was presented in Section 3.1.

The values of geometrical and material parameters, for which both the assumed resonance frequency (145 kHz) and the flat shape of the frequency response curve were obtained (Figure 8), are summarized in Table 3.

Table 3. Parameters of piezoelectric transducer structures optimized using the KLM model.

Parameter	Symbol	Value	Unit
Active layer (piezoelectric ceramic):			
Thickness	d	6.2	Mm
Radius	r	6.35	Mm
Area	A	126.61	mm ²
Acoustic impedance	Z_0	31.0	MRayl
Backing layer ¹ :			
Thickness	d	8.8	Mm
Density	ρ	2546	kg/m ³
Longitudinal velocity	V_L	1790	m/s
Shear velocity	V_S	845	m/s
Acoustic impedance	Z_B	4.56	MRayl
Bulk modulus	K	5.74	GPa
Shear modulus	G	1.82	GPa
Matching layer ² :			
Thickness	d	5.05	Mm
Density	ρ	2079	kg/m ³
Longitudinal velocity	V_L	3029	m/s
Shear velocity	V_S	1640	m/s
Bulk modulus	K	11.62	GPa
Shear modulus	G	5.59	GPa
Acoustic impedance	Z_M	6.3	MRayl

¹ Epoxy/tungsten composite with 0.08 volume fraction of tungsten; ² epoxy/alumina composite with 0.3825 volume fraction of alumina.

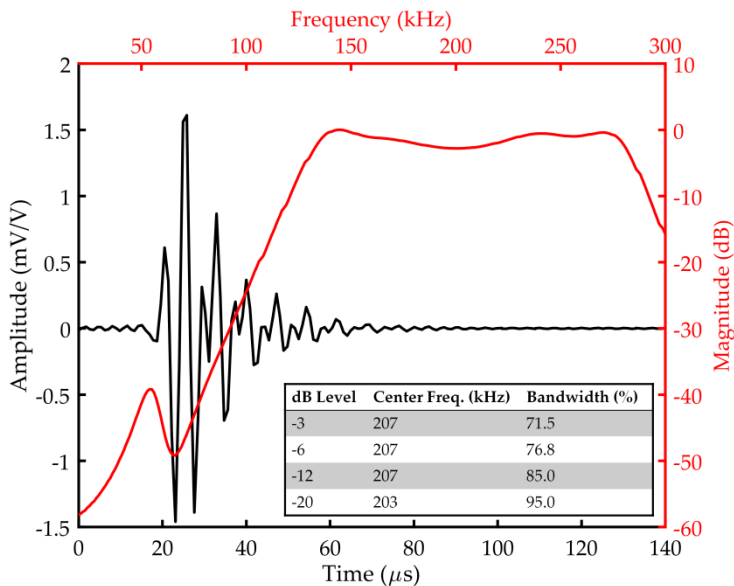


Figure 8. Modeled pulse–echo waveform (black) and frequency spectrum (red) of the transducer with a quarter wavelength matching layer made by an epoxy/alumina composite.

4. Fabrication of a Prototype Active Dielectric Window

4.1. Dielectric Window

The dielectric window was made using extrusion technology with high-strength aluminous porcelain. The parameters are listed in Table 4. This material was chosen according to its numerous advantages, among which the most important were high-temperature resistance, high electrical resistivity, very good chemical resistance to mineral oil, high hardness, easy surface treatment, and low cost of fabrication.

Table 4. Properties of the high-strength aluminous porcelain used to construct the dielectric window.

Parameter	Symbol	Value	Unit
Apparent (bulk) density ¹	ρ_b	2500	kg/m ³
Flexural strength ¹	σ	140	MPa
Fracture toughness ¹	K	2.0	MPa·m ^{1/2}
Young's modulus ¹	E	100	GPa
Abrasion resistance (volume loss)	WV	172	mm ³
Dielectric strength ¹	V_B	20	kV/mm
Resistivity ¹	ρ	10^{13}	$\Omega\cdot\text{cm}$
Thermal shock resistance ¹	T_c	150	K

¹ Minimum values.

In the next stage of the prototype ADW production, four radial holes for piezoelectric transducers were made. The shape of the cross-section and dimensions of the ADW are presented in Figure 9.

Before starting the fabrication of the ultrasonic transducers, the front side of the dielectric window and hole walls were covered with ~1.8–2-mm acoustic insulation layer (Figure 10a). The layer performed the function of an attenuating barrier of both transverse and longitudinal ultrasonic waves as well as transformer tank vibrations, which could excite piezoelectric elements. Polyurethane elastomer was chosen as an attenuating material, because it has very good sound attenuating properties [29–31] as well as high mechanical and thermal durability (Table 5). In order to increase the efficiency of sound attenuation during the mixing of the two components (polyol and isocyanate) of polyurethane together, small air bubbles were intentionally added to the mixture (Figure 10b). This way, a porous material with very good sound attenuating properties was obtained [32,33]. The measurement results

showed that covering the dielectric window with a 2-mm layer of porous polyurethane elastomer caused attenuation of longitudinal waves by 25.47 dB and transversal waves by 24.98 dB on average.

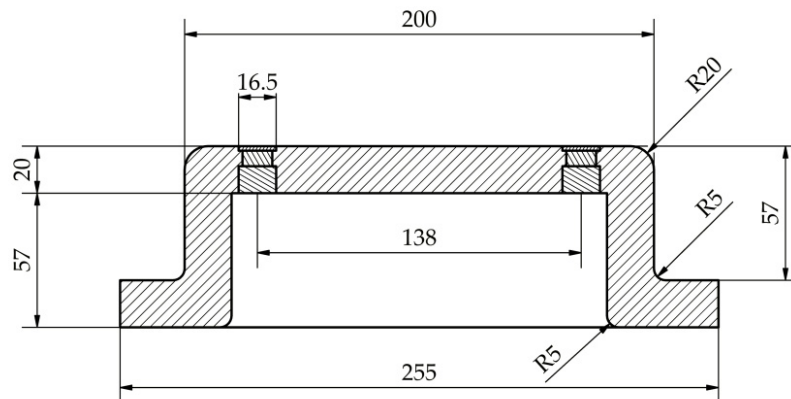


Figure 9. Technical drawing with the dimensions of the prototype active dielectric window.

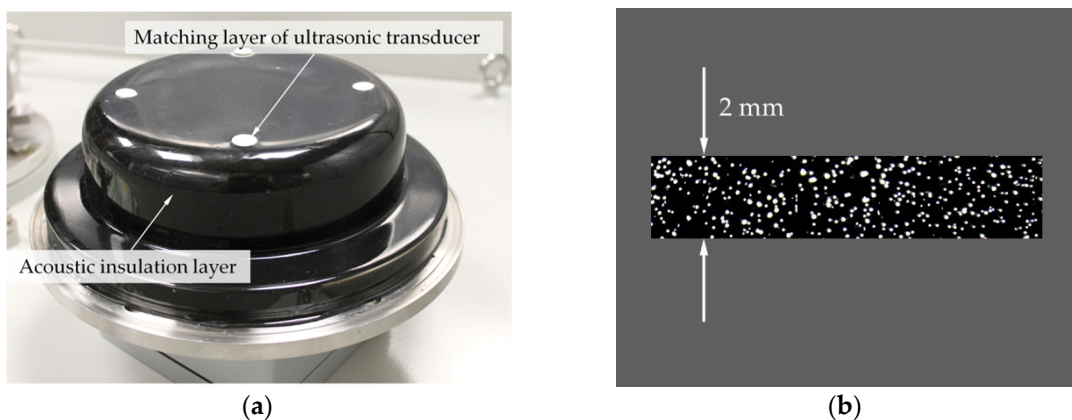


Figure 10. Active dielectric window with acoustic insulation: (a) Photograph of the front part of the ADW covered with a ~2-mm layer of polyurethane elastomer; (b) microscopic photo of the cross-section of a polyurethane sample with air bubbles (visible here as white areas).

Table 5. Mechanical and thermal properties of the polyurethane elastomer used to make the acoustic insulation of the prototype active dielectric window.

Parameter	Symbol	Value	Unit
Elongation at break at 23 °C ¹	ε_B	900	%
Tensile strength at break at 23 °C ¹	σ_B	13	MPa
Tear resistance at 23 °C ²	T_S	54	kN/m
Abrasion resistance ³	A_R	18	mg/100u
Hardness, Shore A ⁴	HSA	85	-
Working temperature	T_W	-40/+90	°C

¹ Acc. to ISO 37; ² acc. to ISO 34; ³ acc. to ISO 5470, Taber abrasion (H22); ⁴ acc. to ISO 868.

4.2. Ultrasonic Transducers

In the next ADW production stage, the main ultrasonic transducer components were placed in previously drilled holes. These components included piezoelectric ceramics and matching and backing layers. The parameters are listed in Table 3. A technical drawing with the dimensions is presented in Figure 11. The prototype was equipped with four piezoelectric ultrasonic transducers, allowing for, besides online PD monitoring, localization of the position of a PD source by estimating the time difference of arrival between registered UHF and AE signals. As was mentioned before, the ADW may also be made in a simplified version for continuous (online) monitoring of partial discharge intensity.

In this configuration, the dielectric window has no acoustic insulation layer and is equipped with only one ultrasonic transducer.

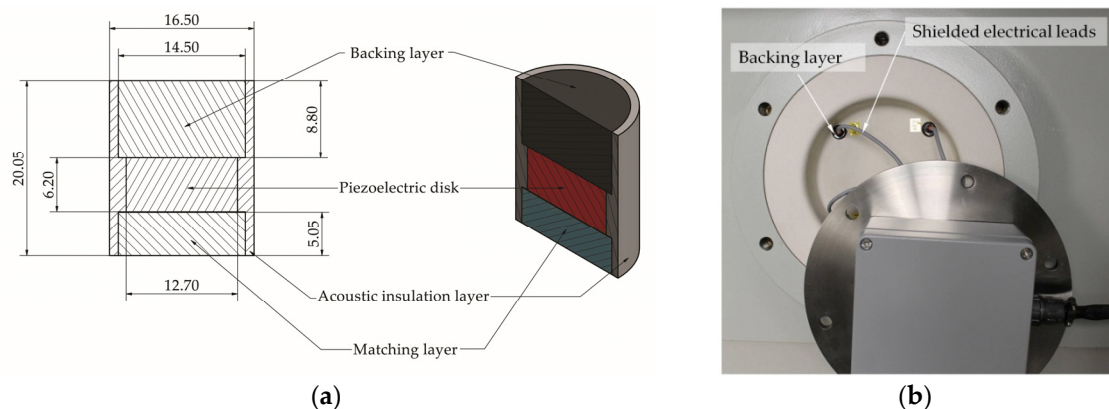


Figure 11. Structural elements of the ultrasonic transducer built into the dielectric window: (a) Technical drawing with the dimensions; (b) photo showing backing layers and electrical leads embedded in the prototype ADW.

Having fabricated the ultrasonic transducers, their calibration was carried out according to the ASTM E976 standard (the so-called “face-to-face” test) [34,35]. Figure 12 presents a typical, representative frequency response curve, the shape of which largely coincides with characteristics predicted by the KLM model (see Figure 8). According to the adopted project assumptions discussed in Section 3.4, a relatively flat curve in the range between ~120 and ~270 kHz was obtained. The central frequency amounted to 195 kHz, whereas the first resonance frequency totaled 134 kHz, which means that it was 10 kHz lower than the one predicted by the KLM model.

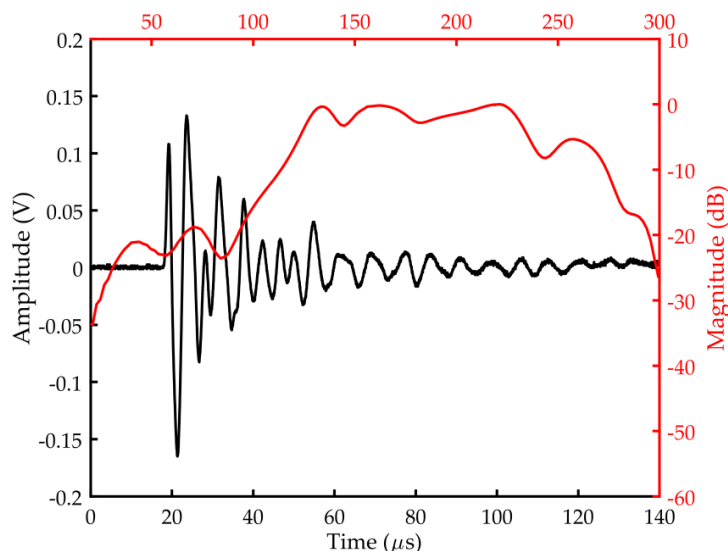


Figure 12. Typical acoustic emission (AE) waveform (black) and frequency response (red) registered during an ultrasonic transducer calibration performed according to the ASTM E976 standard.

4.3. AE Signal Conditioning Unit

In order to design a low-noise AE signal amplifier, in the first stage of design, the analysis of parameters of the newest available on the market operational and instrumentation amplifiers was carried out, and the most important requirements were defined, such as low voltage noise ($<10 \text{ nV}/\sqrt{\text{Hz}}$), simultaneously with high gain ($G \geq 100$), wide bandwidth ($\geq 500 \text{ kHz}$), low current consumption ($<10 \text{ mA}$), and a high common-mode rejection ratio ($\text{CMRR} > 80 \text{ dB}$). Products of the

leading manufacturers currently offering the most advanced electronic components, including Texas Instrument, Analog Devices, Linear Technology, and Maxim Integrated Products, were considered. Eventually, the high-speed instrumentation amplifier AD8421BRZ by Analog Devices (Norwood, USA) was selected. AD8421BRZ is a low-power (2.3 mA maximum supply current), extremely low-noise ($3.2 \text{ nV}/\sqrt{\text{Hz}}$ maximum input voltage), and ultralow bias current ($< 500 \text{ pA}$) instrumentation amplifier specially designed for a broad spectrum of signal conditioning and data acquisition applications. Furthermore, AD8421BRZ is one of the most robust instrumentation amplifiers on the market. It features a high electrostatic discharge (ESD) protection rating of 2 kV human body model (HBM), and overvoltage protection (OVP) of 40 V from the opposite supply rail.

At the instrumentation amplifier output, an active bandpass filter (20–500 kHz) based on Sallen-Key architecture was placed. Both the low- and high-pass sections had the structure of a fourth-order Butterworth filter with unity gain. The ADA4898 (Analog Devices, Norwood, MA, USA) op-amp, belonging to the so-called class of ultralow noise operational amplifiers (noise $< 1 \text{ nV}$ at 100 kHz), was applied as an active element.

At the filter output, the operational amplifier AD813ARZ (Analog Devices, Norwood, MA, USA) performing the function of a voltage follower was applied. Its task was to buffer the output and matching output impedance of the AE signal conditioning unit to the impedance of the coaxial cable (50Ω). Low current consumption (max 8 mA), low voltage noise ($2.9 \text{ nV}/\sqrt{\text{Hz}}$), and wide bandwidth amounting to 80 MHz (3 dB, $G = 1 \text{ V/V}$) were the most significant parameters recognized during the amplifier selection. Moreover, the output of AD813ARZ could drive capacitive loads ($> 1000 \text{ pF}$) directly, without parasitic oscillations. Coaxial cables of high quality are characterized by low capacity (approximately $50\text{--}70 \text{ pF/m}$), and therefore for the signal transmission from the amplifier to the signal acquisition unit one may flawlessly use long cables, even more than ten meters in length.

A schematic diagram of the AE signal conditioning unit and its frequency response curve are presented in Figure 13. The measurement results showed that the level of noise at the output of the measuring channel with 40 dB gain and with connected ultrasonic transducer did not exceed $1.6 \text{ mV}_{\text{p-p}}$.

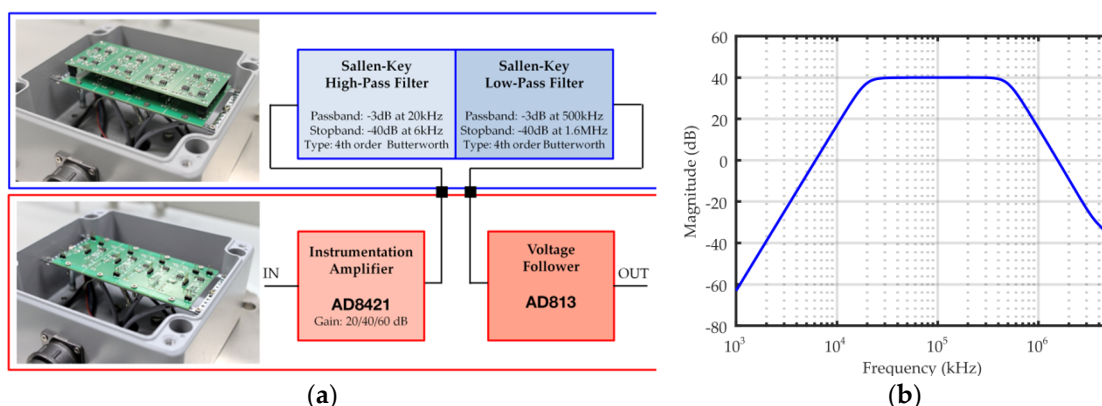


Figure 13. Four-channel AE signal conditioning unit: (a) Schematic diagram with pictures of the fabricated PCB boards; (b) frequency response curve.

4.4. UHF Antenna

While designing the active dielectric window, it was desired to simplify all its components. Therefore, a circular microstrip antenna (CMA) was selected as a radio frequency (RF) detector. This choice was determined by such factors as simple design, low fabrication cost, and ease of assembly in a dielectric window. This antenna type (also called a disk sensor) is commonly applied in online PD monitoring systems for GIS/GIL [17,20,21,36,37]. The limitation of a circular microstrip antenna is relatively low gain and a narrow bandwidth. Therefore, if a first priority is obtaining the highest possible PD detection sensitivity, a CMA may be replaced by one with modern, broadband construction, e.g., a fractal antenna [38,39] or a modified planar inverted-F antenna (PIFA) [40].

A schematic diagram of a circular microstrip antenna fabricated for the prototype ADW is presented in Figure 14.

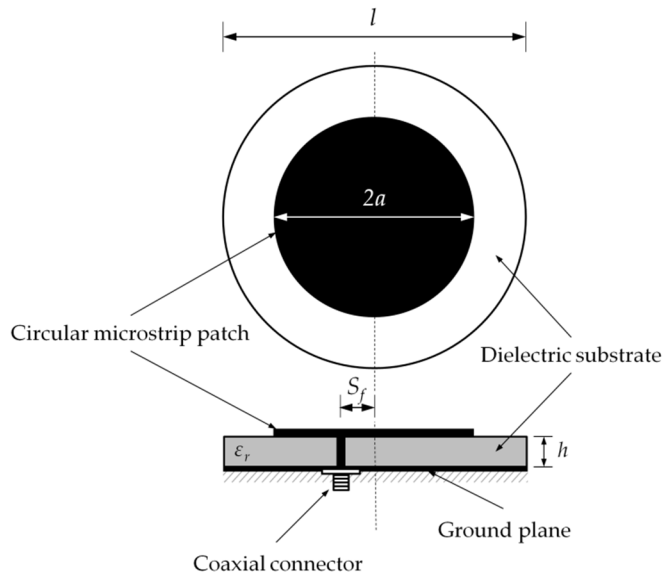


Figure 14. Schematic diagram of a circular microstrip antenna.

The fabrication of the antenna FR-4 laminate was of height $h = 2.45$ mm and relative permittivity $\epsilon_r = 4.4$. The diameter of the ground plane amounted to $l = 120$ mm. The antenna was designed in such a way so that the resonant frequency $f_{r(110)}$ for the dominant TMz110 mode would be equal to 1000 MHz. The radius $a = 41.04$ mm for the circular patch was calculated using Equation (27):

$$a = \frac{F}{\left\{ 1 + \frac{2h}{\pi\epsilon_r F} \left[\ln\left(\frac{\pi F}{2h}\right) + 1.7726 \right] \right\}^{1/2}} \quad (27)$$

where

$$F = \frac{8.791 \times 10^9}{f_r \sqrt{\epsilon_r}} \quad (28)$$

The antenna was fabricated with PCB technology and equipped with a type N connector. The housing was specially designed and manufactured from polytetrafluoroethylene (PTFE). It performs the following tasks: It protects the antenna from accidental damage and corrosion, adequately positions the antenna in the dielectric window, and ensures durable mechanical connection of the antenna with the inspection hatch cover. Figure 15 presents a picture of the antenna and its housing.

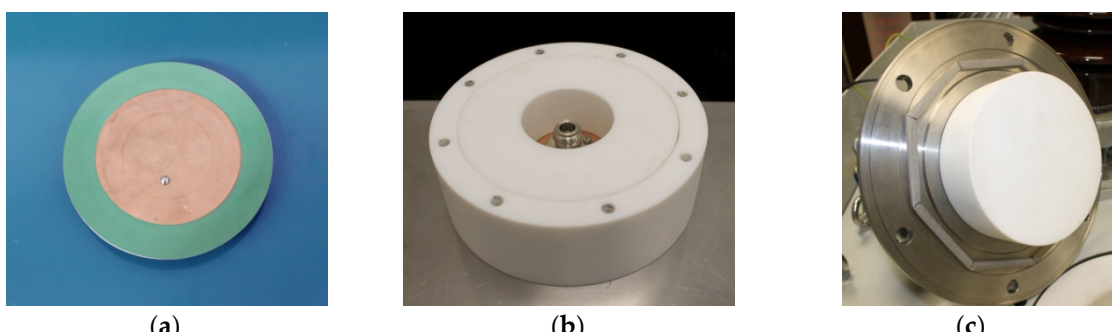


Figure 15. Photos of the fabricated circular microstrip UHF antenna for PD detection: (a) Front view; (b) antenna housing; (c) antenna fixed to the inspection hatch cover.

Having mounted the antenna in the dielectric window, the measurements of the voltage standing wave ratio (VSWR) and input impedance, which allowed confirmation of the proper fabrication of the detector, were carried out. According to the measurement results, the measured resonant frequency $f_{r(110)}$ for the dominant TMz110 mode (Figure 16a) was equal to ~ 1 GHz (exactly 1000.95 MHz). The best impedance matching (very close to $50\ \Omega$) was obtained for the feed point offset $S_f = 14.8$ mm (Figure 16b).

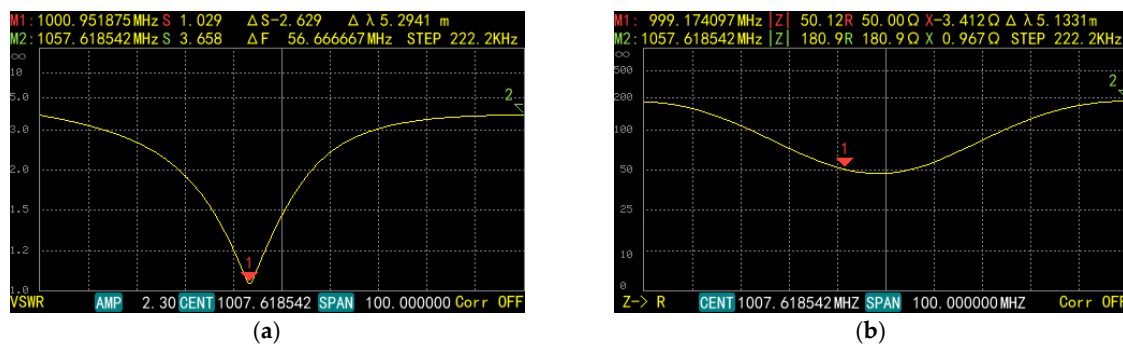


Figure 16. The measured parameters of the fabricated UHF antenna: (a) Voltage standing wave ratio (VSWR); (b) input impedance.

5. Laboratory Tests of the Prototype Active Dielectric Window

5.1. Sensitivity of Detection of AE Waves Generated by PD

An evaluation of the PD detection sensitivity in the ultrasonic range was carried out in a shielded high-voltage laboratory. The oil-filled model of a transformer tank with dimensions $1200 \times 800 \times 750$ mm was used for the investigation (Figure 17a). The modular structure of the tank top cover enabled easy tank configuration adjustment to the selected measurement scenario. The tank may be equipped with maximally five UHF antennas: Two on the top cover, one on the side wall, and two in the oil drain valves (Figure 17b). If necessary, the inspection hatch with a welded flange may be replaced with an ordinary cover (without a hole).

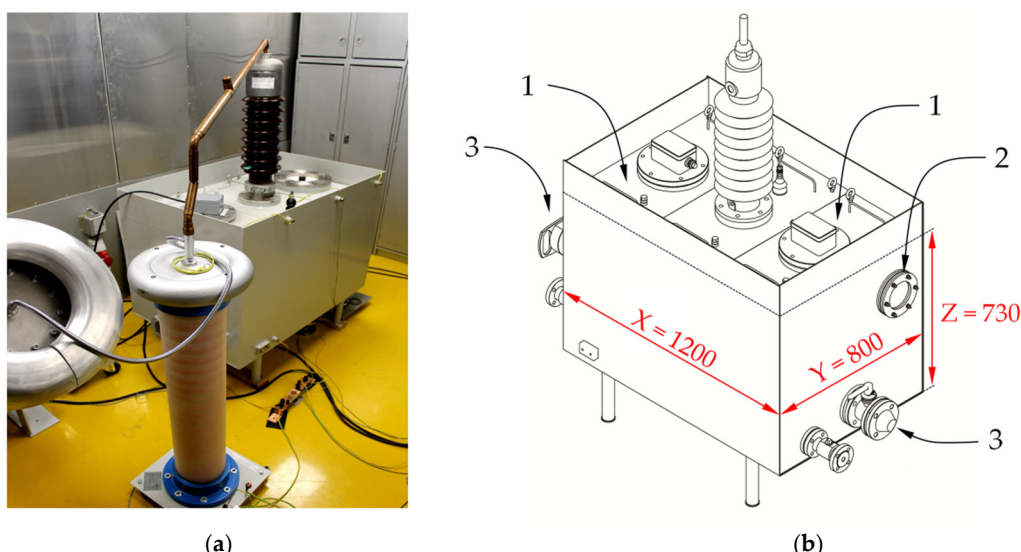


Figure 17. Oil-filled transformer tank: (a) Photograph of the test stand in the shielded high-voltage laboratory; (b) schematic diagram: 1 = inspection hatch with UHF sensors (or plain cover), 2 = inspection hatch with the dielectric window made of poly (methyl methacrylate) (PMMA), 3 = oil drain valve.

An electrode system (Figure 18a), in which the creeping discharges were generated on a pressboard sample with a diameter of 100 mm and a height of 3 mm, was placed in the oil-filled transformer tank (Figure 18b). These types of discharges were selected due to the fact that together with turn-to-turn discharges, they are the most dangerous defects that typically result in catastrophic failures at normal operating conditions [41–45].

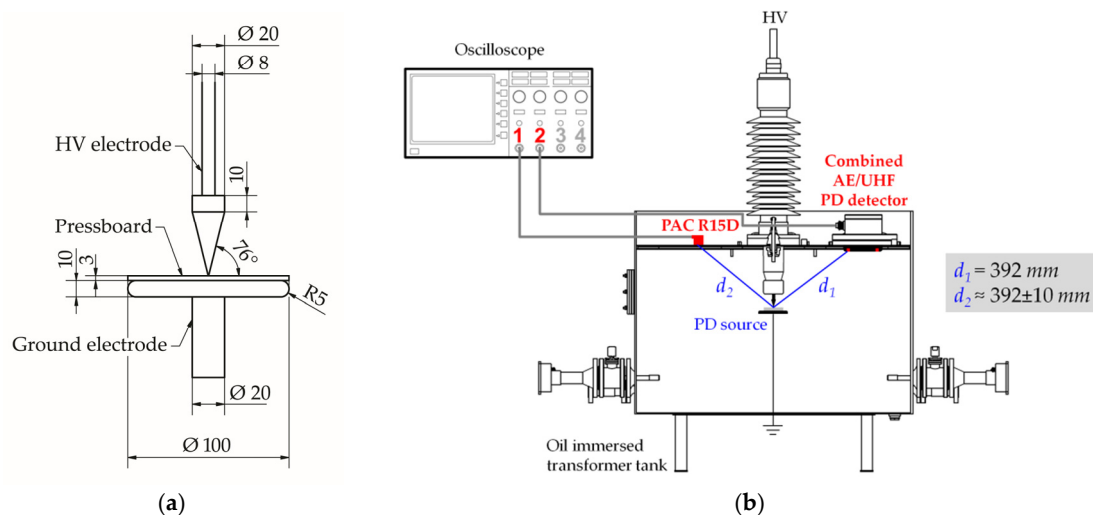


Figure 18. (a) Schematic diagram of the measurement system for evaluating the sensitivity of PD detection in the ultrasound range; (b) electrode system for creeping discharges in oil (PD source).

In order to evaluate the PD detection sensitivity, the AE pulses generated by creeping discharges were registered simultaneously with one of the transducers of the prototype ADW and the reference contact piezoelectric sensor type PAC R15D with 40 dB preamplifier type PAC 2/4/6. Both investigated and referenced ultrasonic transducers were placed 392 mm from the source of discharges (Figure 18a). During the experiment, the level and intensity of PDs were monitored according to the IEC 60270 guidelines using a standard wide-band electrical detector type Doble PD-Smart (Doble Engineering Co, Boston, MA, USA). The inception voltage of creeping discharges amounted to $U_i = 19.6 \text{ kV}$. The AE pulse registration was performed with a voltage of 21.3 kV, at which repeated PD pulses with an average value of apparent charge $q_{avg} = 356 \text{ pC}$ ($q_{max} = 2017 \text{ pC}$) were generated.

The results of the test confirmed, as predicted by the KLM model, a few times higher sensitivity of the ultrasonic transducer optimized for work in transformer oil compared to the popular contact transducer mounted on the transformer tank. A comparative analysis of 250 pairs of AE waveforms showed that the amplitude of the signals registered by the ultrasonic transducer of the ADW was 5.8 times higher on average than that registered by the reference contact transducer PAC R15D. The comparison of the exemplary time waveforms is presented in Figure 19.

5.2. Test of the PD Source Location Using the Active Dielectric Window and TDOA technique

Location of the PD sources in power transformers is usually carried out using the time difference of arrival technique [16,46] or the standard auscultatory technique (SAT) [47]. In addition, research on the application of the direction of arrival (DOA) technique and sensor arrays has been carried out for several years [48–52].

The measurement procedure of TDOA requires using at least four ultrasonic transducers (so-called “all-acoustic measurements”) or replacing one of the ultrasonic transducers with the UHF antenna (so-called “mixed acoustic-electromagnetic measurements”). In this second approach, time differences in acoustic wave arrival to particular AE sensors relative to electromagnetic pulse registered by the UHF antenna are estimated (Figure 20).

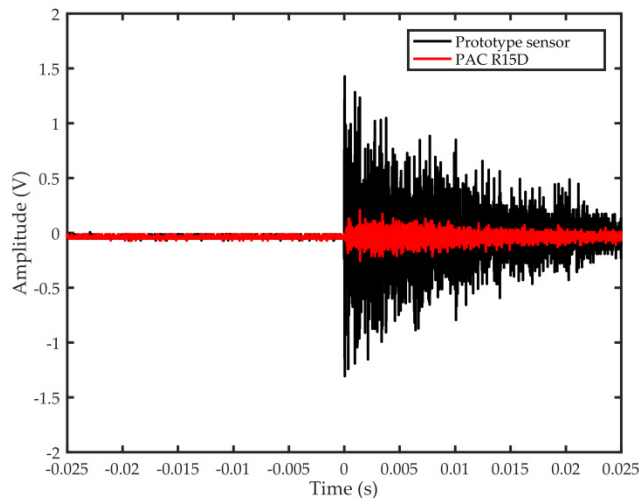


Figure 19. The comparison of the exemplary time waveforms registered by the prototype ultrasonic transducer of the ADW and reference contact piezoelectric transducer type PAC R15D.

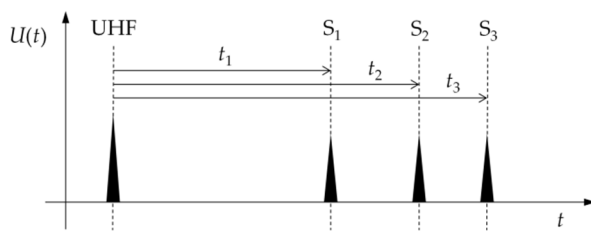


Figure 20. Schematic diagram of the absolute acoustic arrival times (t_1 , t_2 , t_3) to the PD onset (electromagnetic PD trigger signal).

Coordinates (x, y, z) of the PD source are calculated by solving the system of equations below:

$$\begin{aligned} (x - x_{S1})^2 + (y - y_{S1})^2 + (z - z_{S1})^2 &= (v_{oil}t_1)^2 \\ (x - x_{S2})^2 + (y - y_{S2})^2 + (z - z_{S2})^2 &= (v_{oil}t_2)^2, \\ (x - x_{S3})^2 + (y - y_{S3})^2 + (z - z_{S3})^2 &= (v_{oil}t_3)^2 \end{aligned} \quad (29)$$

where x, y, z are unknown PD source coordinates in space; $x_{S1\dots 3}, y_{S1\dots 3}, z_{S1\dots 3}$ are Cartesian coordinates of the AE sensors $S1\dots S3$; t_1, t_2, t_3 are measured absolute arrival times; and v_{oil} is the propagation velocity of acoustic waves in transformer oil. The above nonlinear system of equations can be solved with one of the direct (non-iterative) solver algorithms [53,54] or with a least square iterative algorithm, the efficiency of which strongly depends on the initial values selected by the user [16].

The main reason for incorrect estimation of the coordinates of the PD source results from the assumption that the AE wave arrives at the transducer along the shortest geometric path (direct path in oil) [2,55]. This assumption is true only in the case when the transducer is in front of a defect. In practice, to the transducer first arrives the wave propagating along the shortest acoustic path (fastest path) (Figure 21) [56]. This is due to the different propagation velocities, which were, approximately, $v_{oil} = 1450$ m/s in oil and $v_{steel} = 5100$ m/s in steel, at 30 °C.

The propagation time for the direct path is

$$t = \frac{\sqrt{X^2 + Y^2}}{v_{oil}} \quad (30)$$

and for the fastest path is

$$t = \frac{Y}{v_{oil} \cos \alpha} + \frac{X - Y \tan \alpha}{v_{steel}} \quad (31)$$

where α is the critical incidence angle

$$\alpha = \sin^{-1} \left(\frac{v_{oil}}{v_{steel}} \right) \quad (32)$$

In the case of the prototype ADW, due to the application of an acoustic insulation layer and a remaining oil gap between the dielectric window and the tank, the possibility of structure-borne wave registration was reduced (Figure 22).

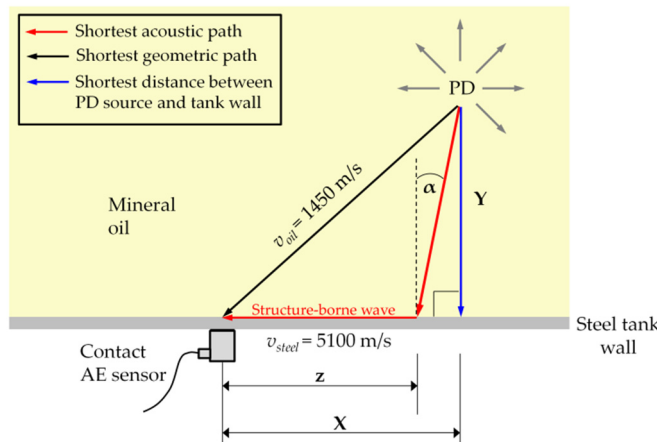


Figure 21. Model of propagation of acoustic waves from the PD source to the contact AE sensor.

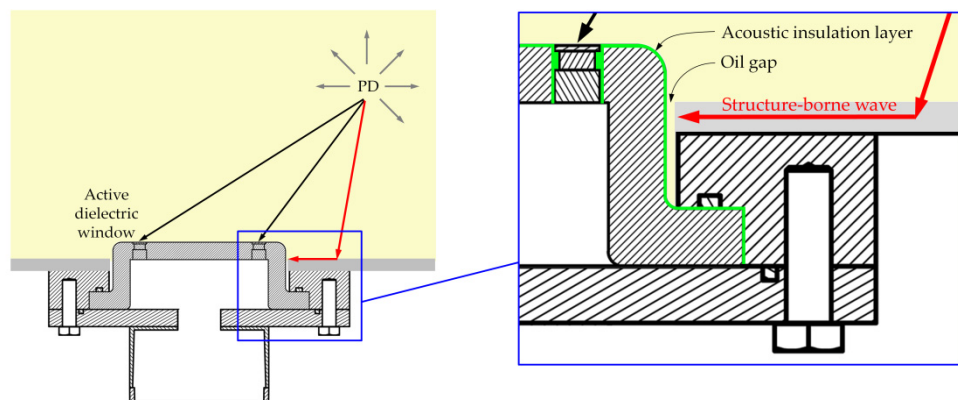


Figure 22. Structural solutions (acoustic insulation layer and oil gap) used in the prototype ADW, reducing the possibility of structure-borne wave registration.

Laboratory research experiments that allowed pre-evaluation of the effectiveness of the location of PD sources using the ADW were carried out in the measurement set-up, the schematic diagram of which is presented in Figure 23. During the investigation, the creeping PDs were generated at the same electrode system as discussed in Section 5.1. The edge of the HV electrode (PD source) was located at the point with coordinates (0.6, 0.4, 0.5). AE signals were registered using three ultrasonic transducers of the active dielectric window with coordinates $S_1(0.924, 0.4, 0.72)$, $S_2(0.996, 0.472, 0.72)$, and $S_3(1.069, 0.4, 0.72)$. Time differences of arrival t_1 , t_2 , t_3 were estimated between the onset of the UHF pulse registered with the circular microstrip antenna and onsets of the AE pulses registered by ultrasonic transducers S_1 , S_2 , and S_3 , respectively. In Figure 24, exemplary time waveforms with marked time differences of arrival of the AE signal to ultrasonic transducers are shown.

Figure 25 presents graphically the obtained results of the PD location, whereas the results of the statistical analysis are shown in Table 6.

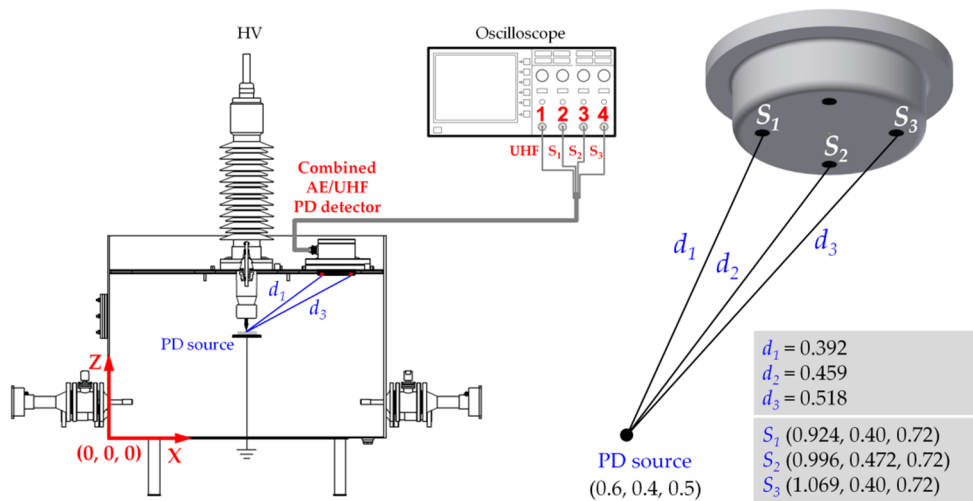


Figure 23. The measurement set-up for testing the effectiveness of a partial discharge source location using the prototype ADW.

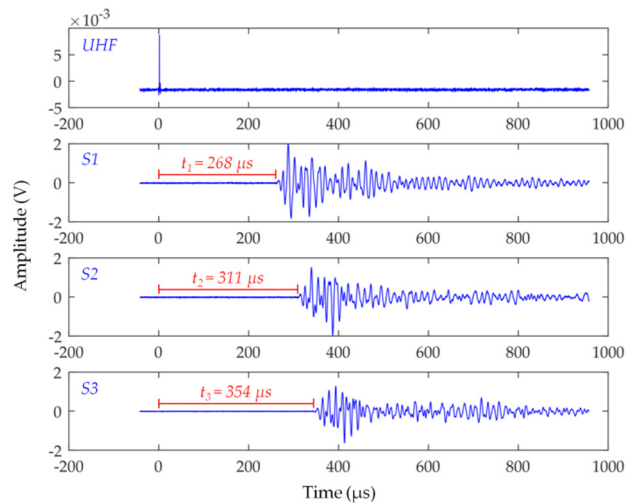


Figure 24. Typical time waveforms with marked time differences of arrival of the AE signal to ultrasonic transducers.

Table 6. Results of PD location obtained using the active dielectric window.

Coordinates	Location of PD Source and Error					
	Actual Location (m)	Calculated Location ¹ (m)	Mean Location Error (cm)	Maximum Location Error (cm)		
					(%)	(%)
X	0.600	0.596	-0.4	0.7	2.0	3.3
Y	0.400	0.407	0.7	1.8	2.8	7.0
Z	0.500	0.485	-1.5	3.0	4.6	9.2

¹ The average value from 100 sets of PD pulses.

The obtained results confirmed the possibility of efficient use of the ADW for the location of PD sources. The average location error did not exceed 1.5 cm (3.0%). For comparison, the standard location, i.e., with a UHF drain valve probe, and three contact piezoelectric sensors of type PAC R15D with coordinates S₁(0.924, 0, 0.36), S₂(0.996, 0, 0.432), and S₃(1.069, 0, 0.36) were performed. Due to that, the location of the contact transducers on the x axis was identical to the transducers in the active dielectric window. A detailed schematic diagram of the measurement set-up configuration is presented in Figure 26. In turn, Figure 27 shows exemplary PD pulses with marked time differences of arrival of the AE signal to contact piezoelectric sensors.

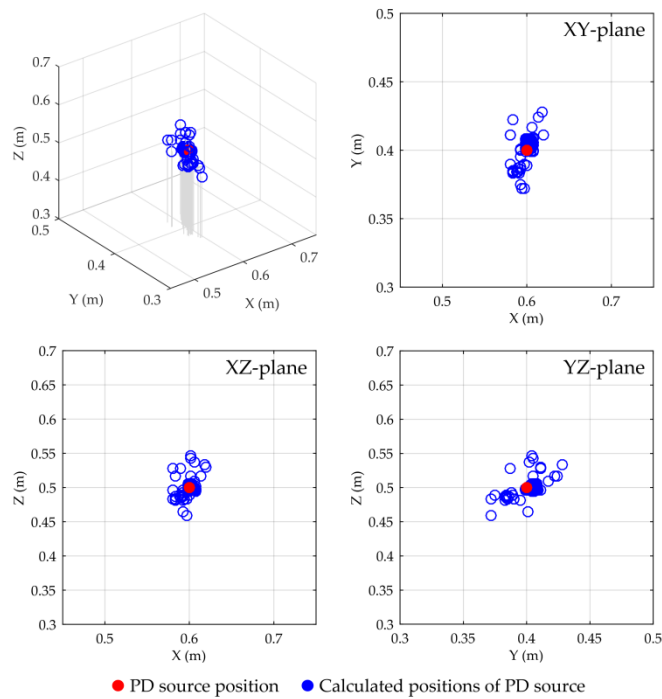


Figure 25. Graphical presentation of the results of PD source location using the prototype active dielectric window: Pseudo-3D plot and projection of solutions on the XY, XZ, and YZ planes.

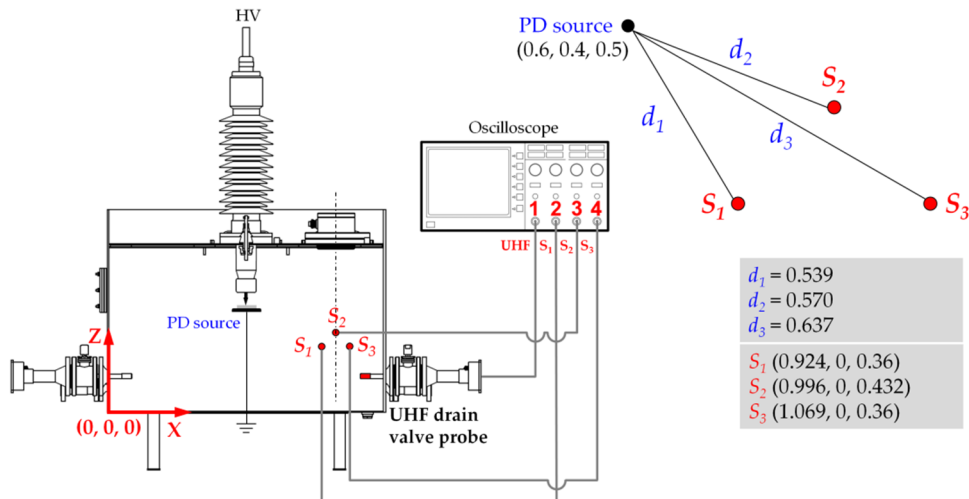


Figure 26. The measurement set-up for testing the effectiveness of partial discharge source location using a UHF drain valve probe and three standard contact piezoelectric sensors.

The obtained results of the PD location are presented in Table 7 and Figure 28. As one may notice, location with the contact transducers was fraught with much higher error. The highest average (20.8%) and maximal (27%) error were observed for the coordinate Z (in the case of the ADW, it was 3% and 9.2%, respectively). Such a large location error was due to the fact that the contact transducers were located at a high angle to the PD source ($> 50^\circ$), and therefore they first registered the ultrasonic wave propagating along the shortest acoustic path, whereas approximately its half went to the steel transformer tank. In turn, AE sensors in the ADW, which worked directly in oil, first registered (according to the TDOA method assumptions) the wave propagating along the shortest path in oil (direct path). It should be emphasized that for very small angles, i.e., when the contact transducers were located almost opposite to the PD source, location errors were small, comparable to ADW.

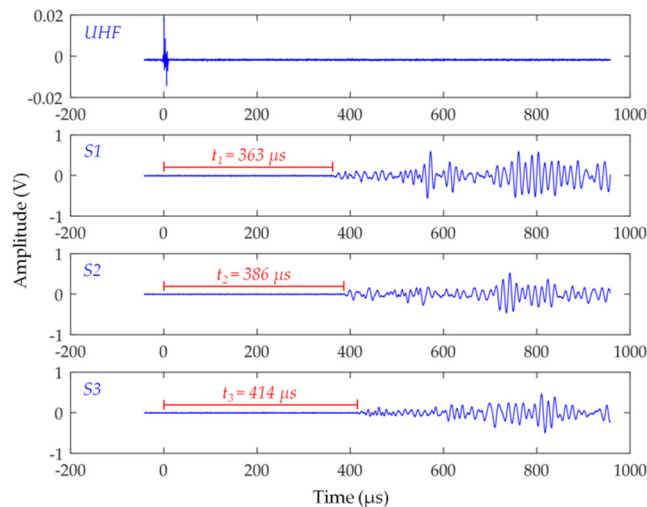


Figure 27. Typical time waveforms with marked time differences of arrival of the AE signal to ultrasonic transducers.

Table 7. Results of the PD location obtained using the active dielectric window.

Coordinates	Location of PD Source and Error					
	Actual Location (m)	Calculated Location ¹ (m)	Mean Location Error (cm)	Maximum Location Error (cm)	Mean Location Error (%)	Maximum Location Error (%)
X	0.600	0.710	11.0	14.8	18.3	24.7
Y	0.400	0.479	7.9	10.7	19.8	26.8
Z	0.500	0.396	-10.4	13.5	20.8	27.0

¹ The average value from 100 sets of PD pulses.

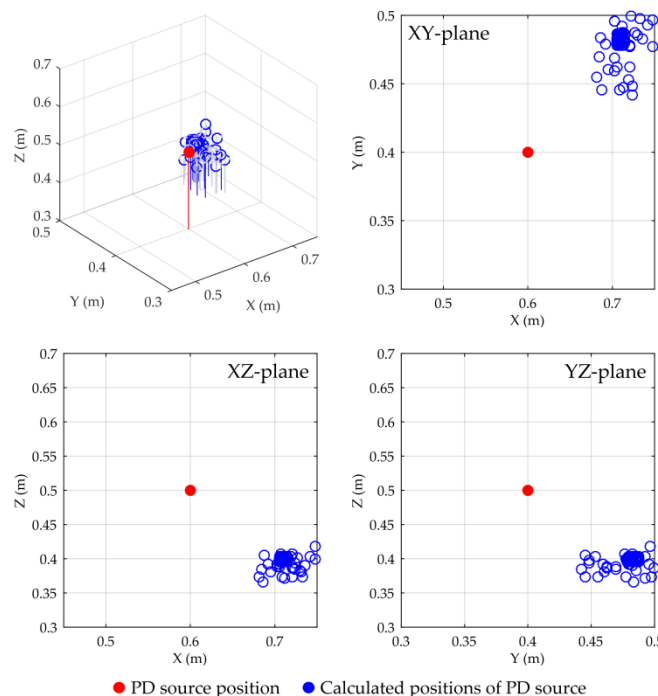


Figure 28. Graphical presentation of the PD source location using a UHF drain valve probe and three piezoelectric contact transducers: Pseudo-3D plot and projection of solutions on the XY, XZ, and YZ planes.

6. Conclusions

This paper presents a new concept of a combined AE/UHF partial discharge detector produced in the form of a dielectric window and designed for assembly in the inspection hatch of a transformer tank. The proposed PD detector, named an active dielectric window, is characterized by a simple design and low fabrication cost. The main innovation of the proposed solution lies in the fact that ultrasonic transducers were built into the dielectric window and optimized for operation in mineral oil. For that reason, the matching layer of ultrasonic transducers was made of specially tailored epoxy/alumina composite with the acoustic impedance equal to the geometric mean of the impedances of transformer oil and piezoelectric ceramics. Such construction facilitated the transfer of the acoustic energy from the liquid medium to the piezoelectric crystal. In effect, it allowed for obtaining a high sensitivity of detection of the AE pulses generated by partial discharges.

Preliminary laboratory tests showed that the amplitude of creeping discharges registered by the ADW was 5.8 higher on average than the amplitude of pulses registered by general purpose contact AE sensors type PAC R15D. The test of the possibility of ADW applications for PD source location using the TDOA technique was similarly positive. Time delays in the acoustic signal arrival to the ultrasonic transducers were measured relative to the UHF signal registered using a circular microstrip antenna placed in the dielectric window. The ADW was designed in a way to maximally limit the possibility of exciting the ultrasonic transducers by the structure-borne waves propagating in a transformer tank wall. This goal was achieved due to the oil gap between the dielectric window and flange, the rubber gasket with sound-attenuating properties, and, most of all, the covering of the window surface with polyurethane acoustic insulation layer.

The results of the laboratory test showed that the average error of the PD location using an ADW amounted to only 3%. For comparison, the measurement with a standard AE system with contact transducers was fraught with an error of over 20%.

Currently, the research, whose aim is to evaluate ADW usefulness in online PD monitoring, is being carried out. In September 2018, two units of ADW were on a pilot basis installed on a power transformer 110 kV/16 kV working in the brown coal mine “Belchatow”. At the same time, research work is being carried out aimed at (1) developing a dielectric window with ultrasound transducers with a lower resonant frequency (approximately 60 kHz (this should guarantee higher sensitivity of detection of high-energy partial discharges)), (2) the construction of a dielectric window using materials with better sound-dampening properties (e.g., porous ceramics or nanoparticle-reinforced polymer composites), and (3) improving the acoustic separation between the piezoelectric element and the dielectric window.

Funding: This work was supported by the Polish National Centre for Research and Development, within the Applied Research Programme, grant No. PBS3/A4/12/2015.

Conflicts of Interest: The author declares no conflicts of interest.

References

1. Sikorski, W.; Ziomek, W. Detection, Recognition and Location of Partial Discharge Sources Using Acoustic Emission Method. In *Acoustic Emission*; Sikorski, W., Ed.; IntechOpen: Rijeka, Croatia, 2012; pp. 49–74. ISBN 978-953-51-0056-0.
2. IEEE Guide for the Detection and Location of Acoustic Emissions from Partial Discharges in Oil-Immersed Power Transformers and Reactors. In *IEEE Std C57.127-2007 (Revision of IEEE Std C57.127-2000)*; IEEE: Piscataway, NJ, USA, 2007. [[CrossRef](#)]
3. Lundgaard, L.E. Partial discharge. XIII. Acoustic partial discharge detection-fundamental considerations. *IEEE Electr. Insul. Mag.* **1992**, *8*, 25–31. [[CrossRef](#)]
4. Bengtsson, T.; Leijon, M.; Ming, L. Acoustic Frequencies Emitted by Partial Discharges in Oil. In Proceedings of the 8th International Symposium on High Voltage Engineering, Yokohama, Japan, 21–23 July 1993; pp. 113–116.

5. Bengtsson, T.; Jönsson, B. Transformer PD diagnosis using acoustic emission technique. In Proceedings of the 10th International Symposium on High Voltage Engineering, Montréal, QC, Canada, 25–29 August 1997; pp. 73–79.
6. Antony, D.; Punekar, G.S. Improvements in AEPD location identification by removing outliers and post processing. In Proceedings of the International Conference on Condition Assessment Techniques in Electrical Systems (CATCON), Bangalore, India, 10–12 December 2015; pp. 66–69. [[CrossRef](#)]
7. Chai, M.L.; Thayoob, Y.H.M.; Ghosh, P.S.; Sha’ameri, A.Z.; Talib, M.A. Identification of Different Types of Partial Discharge Sources from Acoustic Emission Signals in the Time-Frequency Representation. In Proceedings of the International Power and Energy Conference, Putra Jaya, Malaysia, 28–29 November 2006; pp. 581–586. [[CrossRef](#)]
8. Choi, S.-Y.; Park, D.-W.; Kim, I.-K.; Park, C.-Y.; Kil, G.-S. Analysis of acoustic signals generated by partial discharges in insulation oil. In Proceedings of the 2008 International Conference on Condition Monitoring and Diagnosis, Beijing, China, 21–24 April 2008; pp. 525–528. [[CrossRef](#)]
9. Boya, C.; Ruiz-Llata, M.; Posada, J.; Garcia-Souto, J.A. Identification of multiple partial discharge sources using acoustic emission technique and blind source separation. *IEEE Trans. Dielectr. Electr. Insul.* **2015**, *22*, 1663–1673. [[CrossRef](#)]
10. Hoskins, P.R.; Martin, K.; Thrush, A. *Diagnostic Ultrasound: Physics and Equipment*; Cambridge University Press: Cambridge, UK, 2010.
11. IEC-62478. *High-Voltage Test Techniques—Measurement of Partial Discharges by Electromagnetic and Acoustic Methods*; International Electrotechnical Commission (IEC): Geneva, Switzerland, 2016.
12. Walczak, K.; Sikorski, W.; Siodla, K.; Andrzejewski, M.; Gil, W. Online condition monitoring and expert system for power transformers. In Proceedings of the 3rd Advanced Research Workshop on Transformers, Santiago de Compostella, Spain, 3–10 October 2010; pp. 433–438.
13. Sikorski, W.; Walczak, K.; Moranda, H.; Gil, W.; Andrzejewski, M. Partial discharge on-line monitoring system based on acoustic emission method—Operational experiences. *Prz. Elektrotech.* **2012**, *88*, 117–121.
14. Albaracín, R.; Ardila-Rey, J.A.; Mas’ud, A.A. On the Use of Monopole Antennas for Determining the Effect of the Enclosure of a Power Transformer Tank in Partial Discharges Electromagnetic Propagation. *Sensors* **2016**, *16*, 148. [[CrossRef](#)] [[PubMed](#)]
15. Fofana, I.; Hadjadj, Y. Electrical-Based Diagnostic Techniques for Assessing Insulation Condition in Aged Transformers. *Energies* **2016**, *9*, 679. [[CrossRef](#)]
16. Markalous, S.; Tenbohlen, S.; Feser, K. Detection and location of partial discharges in power transformers using acoustic and electromagnetic signals. *IEEE Trans. Dielectr. Electr. Insul.* **2008**, *15*, 1576–1583. [[CrossRef](#)]
17. Unsworth, J. Partial Discharge Monitoring System for Transformers. U.S. Patent Grant No. US6774639B1, 2 September 1999.
18. Unsworth, J.; Kurusingal, J.; James, R.E. On-line partial discharge monitor for high voltage power transformers. In Proceedings of the 4th International Conference on Properties and Applications of Dielectric Materials (ICPADM), Brisbane, Australia, 3–8 July 1994; Volume 2, pp. 729–732. [[CrossRef](#)]
19. Siegel, M.; Beltle, M.; Tenbohlen, S.; Coenen, S. Application of UHF sensors for PD measurement at power transformers. *IEEE Trans. Dielectr. Electr. Insul.* **2017**, *24*, 331–339. [[CrossRef](#)]
20. Judd, M.D.; Farish, J.S.; Pearson, J.S.; Hampton, B.F. Dielectric windows for UHF partial discharge detection. *IEEE Trans. Dielectr. Electr. Insul.* **2001**, *8*, 953–958. [[CrossRef](#)]
21. Judd, M.D.; Farish, J.S.; Hampton, B.F. Broadband couplers for UHF detection of partial discharge in gas-insulated substations. *IEE Proc. Sci. Meas. Technol.* **1995**, *142*, 237–243. [[CrossRef](#)]
22. CIGRE. *Experiences in Service with New Insulating Liquids*; CIGRE Brochure N° 436; CIGRE: Paris, France, 2010.
23. Nadolny, Z.; Dombek, G. Electro-Insulating Nanofluids Based on Synthetic Ester and TiO₂ or C₆₀ Nanoparticles in Power Transformer. *Energies* **2018**, *11*, 1953. [[CrossRef](#)]
24. Li, P.; Dai, K.; Zhang, T.; Jin, Y.; Liu, Y.; Liao, Y. An Accurate and Efficient Time Delay Estimation Method of Ultra-High Frequency Signals for Partial Discharge Localization in Substations. *Sensors* **2018**, *18*, 3439. [[CrossRef](#)] [[PubMed](#)]
25. Mason, W.P. *Electromechanical Transducers and Wave Filters*, 2nd ed.; Van Nostrand: Princeton, NJ, USA, 1948; ISBN 9780442051648.

26. Redwood, M. Transient performance of a piezoelectric transducer. *J. Acoust. Soc. Am.* **1961**, *33*, 527–536. [[CrossRef](#)]
27. Krimholtz, R.; Leedom, D.A.; Mattheei, G.L. New equivalent circuits for elementary piezoelectric transducers. *Electron. Lett.* **1970**, *6*, 398–399. [[CrossRef](#)]
28. Devaney, A.J.; Levine, H. Effective elastic parameters of random composites. *Appl. Phys. Lett.* **1980**, *37*, 377–379. [[CrossRef](#)]
29. Imai, Y.; Asano, T. Studies of acoustical absorption of flexible polyurethane foam. *J. Appl. Polym. Sci.* **1982**, *27*, 183–195. [[CrossRef](#)]
30. Herrington, R.; Broos, R.; Knaub, P. Flexible Polyurethane Foams. In *Handbook of Polymeric Foams and Foam Technology*, 2nd ed.; Klempner, D., Sendjarevic, V., Eds.; Hanser Publishers: Munich, Germany, 2004; pp. 55–119, ISBN-13: 978-1569903360.
31. Andersson, A.; Lundmark, S.; Magnusson, A.; Maurer, F.H.J. Vibration and acoustic damping of flexible polyurethane foams modified with a hyperbranched polymer. *J. Cell. Plast.* **2010**, *46*, 73–93. [[CrossRef](#)]
32. Doutres, O.; Atalla, N.; Dong, K. Effect of the microstructure closed pore content on the acoustic behavior of polyurethane foams. *J. Appl. Phys.* **2011**, *110*, 239–246. [[CrossRef](#)]
33. Hong, Z.; Bo, L.; Guangsu, H. Sound absorption behavior of multiporous hollow polymer micro-spheres. *Mater. Lett.* **2006**, *60*, 3451–3456. [[CrossRef](#)]
34. ASTM E976-10 Standard Guide for Determining the Reproducibility of Acoustic Emission Sensor Response; ASTM International: West Conshohocken, PA, USA, 2016; 7p.
35. Ono, K. Calibration Methods of Acoustic Emission Sensors. *Materials* **2016**, *9*, 508. [[CrossRef](#)]
36. Hoshino, T.; Maruyama, S.; Ohtsuka, S.; Hikita, M.; Wada, J.; Okabe, S. Sensitivity comparison of disc- and loop-type sensors using the UHF method to detect partial discharges in GIS. *IEEE Trans. Dielectr. Electr. Insul.* **2012**, *19*, 910–916. [[CrossRef](#)]
37. Pearson, J.S.; Farish, O.; Hampton, B.F.; Judd, M.D.; Templeton, D.; Pryor, B.W.; Welch, I.M. Partial discharge diagnostics for gas insulated substations. *IEEE Trans. Dielectr. Electr. Insul.* **1995**, *2*, 893–905. [[CrossRef](#)]
38. Sikorski, W.; Szymczak, C.; Siodla, K.; Polak, F. Hilbert curve fractal antenna for detection and on-line monitoring of partial discharges in power transformers. *Eksplotat. I Niegawodn. Maint. Reliab.* **2018**, *20*, 343–351. [[CrossRef](#)]
39. Li, J.; Li, X.; Du, L.; Cao, M.; Qian, G. An Intelligent Sensor for the Ultra-High-Frequency Partial Discharge Online Monitoring of Power Transformers. *Energies* **2016**, *9*, 383. [[CrossRef](#)]
40. Szymczak, C.; Sikorski, W.; Siodla, K.; Grobia, M. Design of PIFA-type UHF antenna for partial discharge monitoring in power transformer. *Prz. Elektrotech.* **2018**, *94*, 138–142. (In Polish) [[CrossRef](#)]
41. Sokolov, V.; Berler, Z.; Rashkes, V. Effective methods of assessment of insulation system conditions in power transformers: A view based on practical experience. In Proceedings of the Electrical Insulation Conference and Electrical Manufacturing and Coil Winding Conference (Cat. No.99CH37035), Cincinnati, OH, USA, 28 October 1999; pp. 659–667. [[CrossRef](#)]
42. Liao, R.; Hu, E.; Yang, L.; Duan, L. The process of creeping discharge-caused damage on oil/pressboard insulation. *Turk. J. Electr. Eng. Comput. Sci.* **2016**, *24*, 1434–1445. [[CrossRef](#)]
43. Rozga, P.; Stanek, M.; Pasternak, B. Characteristics of Negative Streamer Development in Ester Liquids and Mineral Oil in a Point-To-Sphere Electrode System with a Pressboard Barrier. *Energies* **2018**, *11*, 1088. [[CrossRef](#)]
44. Sikorski, W.; Walczak, K.; Przybylek, P. Moisture Migration in an Oil-Paper Insulation System in Relation to Online Partial Discharge Monitoring of Power Transformers. *Energies* **2016**, *9*, 1082. [[CrossRef](#)]
45. Dombek, G.; Gielniak, J.; Wroblewski, R. Fire safety and electrical properties of mineral oil/synthetic ester mixtures. In Proceedings of the 2017 International Symposium on Electrical Insulating Materials (ISEIM), Toyohashi, Japan, 11–15 September 2017; pp. 227–230. [[CrossRef](#)]
46. Sikorski, W.; Walczak, K. Power Transformer Diagnostics Based on Acoustic Emission Method. In *Acoustic Emission—Research and Applications*; Sikorski, W., Ed.; IntechOpen: Rijeka, Croatia, 2013; pp. 91–116. ISBN 978-953-51-1015-6.
47. Sikorski, W.; Siodla, K.; Moranda, H.; Ziomek, W. Location of partial discharge sources in power transformers based on advanced auscultatory technique. *IEEE Trans. Dielectr. Electr. Insul.* **2012**, *19*, 1948–1956. [[CrossRef](#)]
48. Luo, Y.F.; Li, Y.M.; Liu, L.C. Simulation of PD location method in oil based on UHF and ultrasonic phased array receiving theory. *Trans. China Electrotech. Technol. Soc.* **2004**, *19*, 35–39.

49. Polak, F.; Sikorski, W.; Siodla, K. Location of partial discharges sources using sensor arrays. In Proceedings of the 2014 International Conference on High Voltage Engineering and Application (ICHVE), Poznan, Poland, 8–11 September 2014; pp. 1–4. [[CrossRef](#)]
50. Xie, Q.; Cheng, S.; Lü, F.; Li, Y. Location of partial discharge in transformer oil using circular array of ultrasonic sensors. *IEEE Trans. Dielectr. Electr. Insul.* **2013**, *20*, 1683–1690. [[CrossRef](#)]
51. Gao, S.; Zhang, Y.; Xie, Q.; Kan, Y.; Li, S.; Liu, D.; Lü, F. Research on Partial Discharge Source Localization Based on an Ultrasonic Array and a Step-by-Step Over-Complete Dictionary. *Energies* **2017**, *10*, 593. [[CrossRef](#)]
52. Yongfen, L.; Xiaohu, X.; Fei, D.; Xiao, T.; Yanming, L. Comparison of DOA Algorithms Applied to Ultrasonic Arrays for PD Location in Oil. *IEEE Sens. J.* **2015**, *15*, 2316–2323. [[CrossRef](#)]
53. Awange, J.L.; Grafarend, E.W. Algebraic solution of GPS Pseudo-Ranging Equations. *GPS Solut.* **2002**, *5*, 20–32. [[CrossRef](#)]
54. Krause, L.O. A direct solution to GPS-type navigation equations. *IEEE Trans. Aerosp. Electron. Syst.* **1987**, *AES-23*, 225–232. [[CrossRef](#)]
55. Lundgaard, L.E. Partial discharge. XIV. Acoustic partial discharge detection—Practical application. *IEEE Electr. Insul. Mag.* **1992**, *8*, 34–43. [[CrossRef](#)]
56. Phung, B.T.; Blackburn, T.R.; Liu, Z. Acoustic measurements of partial discharge signals. *J. Electr. Electron. Eng.* **2001**, *21*, 41–47.



© 2018 by the author. Licensee MDPI, Basel, Switzerland. This article is an open access article distributed under the terms and conditions of the Creative Commons Attribution (CC BY) license (<http://creativecommons.org/licenses/by/4.0/>).